A COMPUTATIONAL FLUID DYNAMICS STUDY ON THE ACCURACY OF HEAT TRANSFER FROM A HORIZONTAL CYLINDER INTO QUIESCENT WATER

William Logie and Elimar Frank

Institut für Solartechnik SPF, 8640 Rapperswil (Switzerland)

1. Introduction

The discipline of prototyping and designing parts or components via direct numerical simulation offers engineers today a powerful tool in the understanding of physical problems. The manipulation and operation of numerical fields representing the conditions we wish to consider (for example by way of Newtonian fluid physics) provides insight and comparative confidence in decisions otherwise grounded on experience or experimental data. To gain this confidence however - that the model parameters and numerical solver are realistic - we must be stringent in their validation for any given problem.

Illustrated in this paper is such a validation for free convective heat transfer (Nusselt number) from a horizontal cylinder into quiescent water. The fluid properties and free convective range of application reflect those occurring within Solar Domestic Hot Water (SDHW) storages with helically coiled Immersed Heat Exchangers (IHX). Once the solver parameters are approved as discussed here, models representing such SDHW storages may be parameterised for simulation under a suitable optimisation cost function.

2. Investigations

For these investigations the open-source Field Operation And Manipulation C++ Toolbox OpenFOAM® was used; specifically, its incompressible solver for free convective heat transfer utilising the Pressure-Implicit with Splitting of Operators (PISO) algorithm under the Boussinesq approximation. By this method, all change in density (effective kinematic density ρ_k) is prescribed by change in temperature (volumetric expansion β) via Eq. (1):

$$\rho_k = 1 - \beta(T - T_0) \tag{1}$$

First the velocity (U) and temperature (T) fields are solved using the hydrostatic pressure ($P_{\rho gh}$[1]) field from the previous time-step before the pressure-implicit loop is called for the current one. The relevant solver parameters and thermo-physical properties for water are given in Table 1.

Table 1: Simulation parameters and nomenclature.

Property	Nomenclature	Value	Units
Solver tolerance for $P_{\rho gh}$	-	1×10^{-8}	$m^2.s^{-2}$
Solver tolerance for U, T, k and ε	-	1×10^{-6}	$m.s^{-1}$, K, $m^2.s^{-2}$ and $m^2.s^{-3}$
Reference/Quiescent Temperature	T_0	293.15	K
Kinematic Viscosity	ν	1.004e-6	$m^2.s^{-1}$
Thermal expansion coefficient	β	207e-6	K^{-1}
Laminar Prandtl Number	Pr	7	-
Thermal Capacitance	C_p	4183	$m^2.s^{-2}.K^{-1}$ ($J.kg^{-1}.K^{-1}$)
Density	ρ	998	$kg.m^{-3}$
Thermal conductivity	$k_f = C_p \rho \nu / \mathrm{Pr}$	0.6	$kg.m.s^{-3}.K^{-1}$ ($W.m^{-1}.K^{-1}$)
Gravity	g	9.81	$m.s^{-2}$

[1] Subscript explanation: $\rho_k \times g \times$ height.

Given that a horizontally orientated cylinder is more or less homogenous in the dimension of its extrusion, the problem can be minimised to be 2 dimensional (see Figure 1).

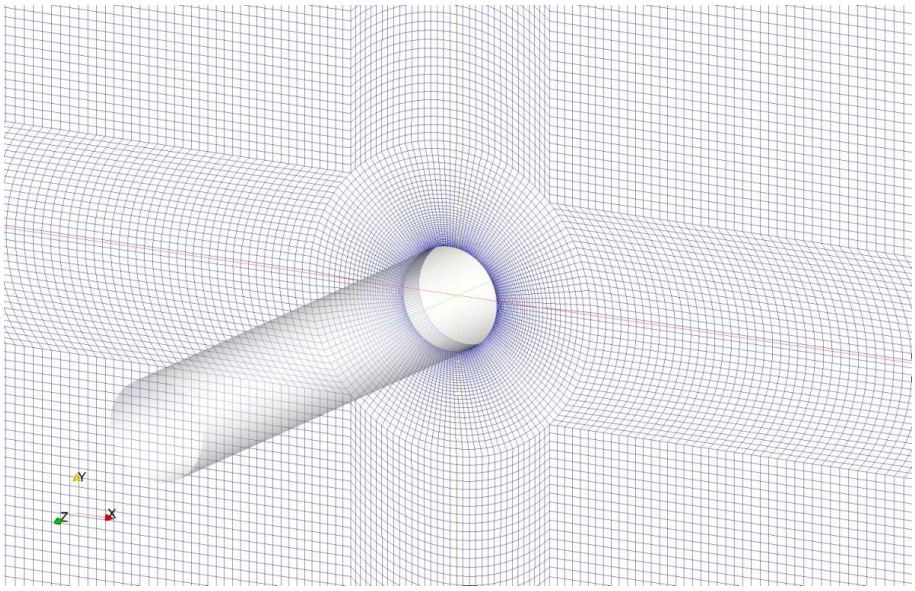

Figure 1: A trimetric view of the hexahedral mesh[2] around the cylinder (parameterised with Gmsh[3]).

The quiescent approximation is achieved by a mesh extending 50cm above and below and 100cm to the right and left of the cylinder walls with Neumann boundary conditions applied to velocity and pressure. This stipulates the derivative a solution is to have when crossing the boundary (in this case zero). An exception was made for pressure at the bottom boundary condition where a *total pressure* was applied so as to provide a reference for the hydrostatic pressure field. The temperature of any fluid entering the mesh is that of the reference temperature and was applied by way of the derived inlet/outlet boundary condition; fixed value entering (Derichlet) and zero gradient exiting (Neumann).

The information sought in this discretised space is contained within the boundary layer around the cylinder; namely the temperature gradient from its surface looking into quiescent water. To obtain an approximation of its logarithmic nature while remaining within realistic numerical scales, an inflation layer was generated whereby the cells increase in size from the cylinder surface towards free fluid. One of the most challenging parts of mesh definition is treatment of the *law of the wall*, where the Reynolds averaging simulation of turbulence in the flow field must be considered together with the viscous sub-layer near the wall. Based on best practice recommendations (Patel et al., 1985) the Launder Sharma low-Reynolds k-ε-turbulence model was applied for flow field angular momentum and dissipation, a dimensionless wall distance y^+ at or below 1.0 was ensured and zero-turbulence at the cylinder wall was fixed. Accordingly, the smallest cell thickness at the cylinder surface was set to $\sim 2\times10^{-4}$ metres and an inflation layer 2 times the radius of the cylinder with a growth factor of 1.1 was applied. This allows for turbulence in the free convective plume erupting from the cylinder while also ensuring direct numerical evaluation of the thermal boundary layer.

Although under the boundary conditions defined a steady state flow can be expected, transient simulations were performed such that the emergence of turbulent phenomena might be observed. Simulations for varying temperature differences (between cylinder surface and quiescent water) and cylinder sizes were run for 1000 seconds, within which time a convergence to quasi-steady state flow always occurred.

We begin with the definition of the average Nusselt number as the integral of the *dimensionless temperature gradient* over the arc length of the cylinders surface as in Eq. (2).

[2] OpenFOAM always operates in a 3D Cartesian coordinate system - 2D geometries consist of a mesh 1 cell thick, normal to which no solution is sought. An advantage of this is that the solver and post-processing algorithms one develops are the same regardless of whether 2D or 3D is simulated.

[3] http://geuz.org/gmsh/

$$\overline{\mathrm{Nu}_D} \equiv \frac{\bar{h}D}{k_f} = \int_0^{2\pi} \left.\frac{\partial T^*}{\partial n^*}\right|_{n^*=0} d\theta \tag{2}$$

Where $\bar{h}$ is the average convection coefficient, D is the cylinder diameter, k_f is the thermal conductivity of the fluid and θ is the angular coordinate around the cylinder. The non-dimensional variables for temperature T^* and length normal to the cylinder surface[4] n^* are given in Eq. (3).

$$T^* = \frac{T - T_0}{T_S - T_0}$$
$$n^* = \frac{n}{D} \tag{3}$$

The temperature subscript S refers to cylinder surface and Figure 2 gives an example of n.

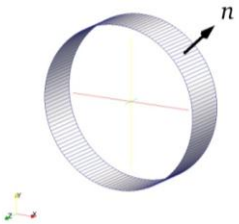

Figure 2: Discretised cylinder surface showing the normal vector *n* for a surface element.

Post processing of the discretised cylinder surface was performed by reworking the relations described in Eqs. (2) and (3) around the wall heat flux q''. This was obtained via the cylinder surface normal temperature gradient with Eq. (4).

$$q'' = k_f \left.\frac{\partial T}{\partial n}\right|_{n=0} \tag{4}$$

From this we can derive the convection coefficient via Eq. (5) and subsequently the local Nusselt number analogously to Eq. (2). Averages were then weighted according to surface element size.

$$h = \frac{q''}{T_S - T_0} \tag{5}$$

The variation of average Nusselt numbers in the buoyant range of ~10^5 < Ra < ~10^8 is compared with two common empirical equations - e.g. from Incropera et al. (2006) or VDI (2010) - namely those from Churchill & Chu (1975) and Morgan (1975).

3. Results

A significant effort has been made to ensure that the computational results are independent of spatial and temporal resolutions. For any given mesh resolution an adaptive time stepping was used such that no cell exchanged more than half of its contents with a neighbour at any time.

Of primary concern regarding accuracy is that all fluid properties remain constant under the Boussinesq approximation. Although this can be compensated for at most by defining fluid properties for each simulation reflecting the average film temperature between cylinder surface and quiescent fluid and adjusting properties (e.g. density) in a post-processing step, it was decided to keep all thermo-physical properties constant for simplicity's sake because we are primarily interested in the comparison.

We can begin by observing the development of the Nusselt number in each simulation of constant

[4] This is not to be confused with y^+ (compare Eq. (3) with http://www.cfd-online.com/Wiki/Dimensionless_wall_distance_(y_plus)).

temperature difference for a cylinder with a diameter of 35mm. In Figure 3 we can see how the local Nusselt number varies over the cylinder surface when ΔT = 10K; from a maximum (32.2) at the bottom where quiescent water separates to a minimum (7.7) at the top where the buoyant flow recombines – the average Nusselt number is 25.7.

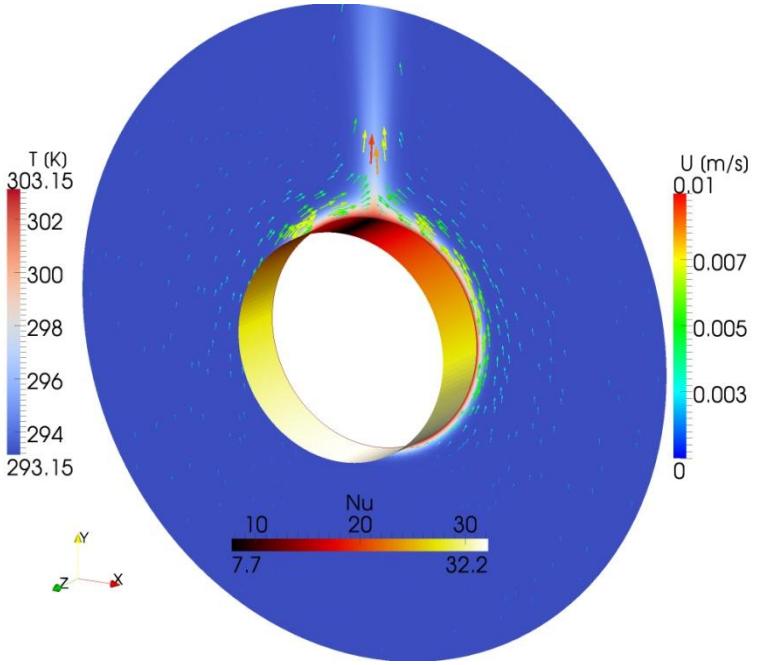

Figure 3: Visualisation of the flow separation and recombination around the cylinders circumference, the temperature field and the local Nusselt number for a cylinder with diameter 35mm and ΔT = 10K.

In Figure 4 the transient response of heat transfer for the first 500 seconds for 6 temperature differences is shown. At the beginning of each run there is no fluid flow; heat transfer is dominated by conduction across a very steep gradient. Feedback between the boundary layer and buoyancy finds equilibrium thereafter and heat transfer stabilises. The water rising in a plume from the cylinder exits the top of the mesh and is replaced from all sides (mostly bottom) by water at the reference temperature – steady-state is thus reached. A mild bump in the Nusselt number is observed at the point in each simulation where the buoyant plume exits the top boundary condition, after which eddies occur ($\Delta T \geq$ 2K) which create fluctuations in the heat transfer response (Figure 5).

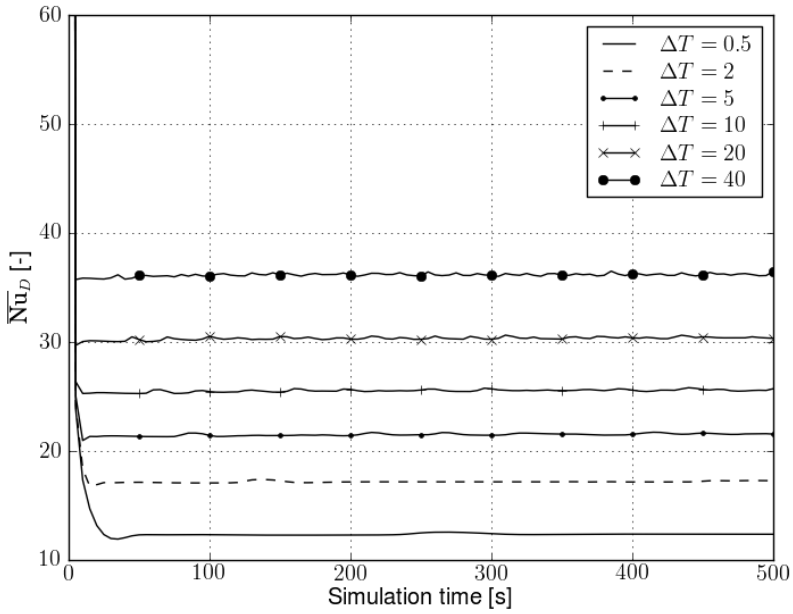

Figure 4: Transient heat transfer response for a cylinder with a diameter of 35mm for varying temperature differences.

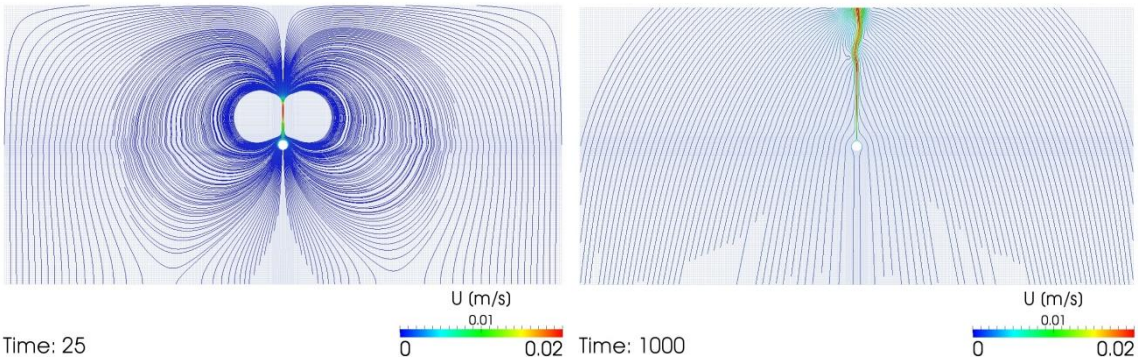

Figure 5: Streamline images showing an initial (left) and a final (right) flow field – cylinder diameter is 35mm and ΔT = 10K.

Plotting the steady state Nusselt numbers against the respective temperature differences (Figure 6) we can compare the numerical results with the correlations from Morgan and Churchill & Chu. The correlation from Morgan divides the relevant Rayleigh range (10^{-10} < Ra < 10^{12}) into five zones with respective constants, whereas Churchill & Chu created two correlation functions; one valid for the entire Rayleigh range and one valid only for the laminar regime (10^{-10} < Ra < 10^{9}).

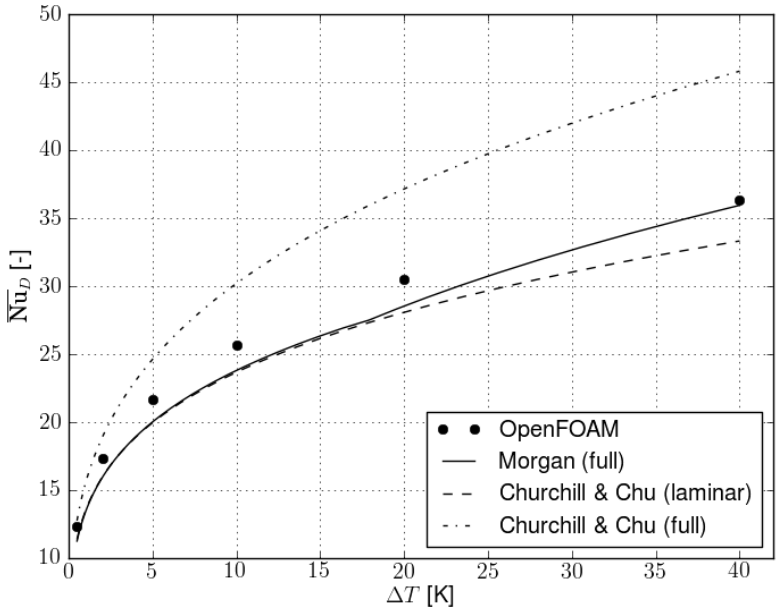

Figure 6: Plot of the average Nusselt number against temperature difference between cylinder surface and quiescent water for a cylinder diameter of 35mm.

The same results plotted onto an axis showing the Rayleigh number are shown in Figure 7, this time including the simulations for cylinder diameters of 20mm and 50mm. It becomes obvious that all simulations remain laminar, a fact that is confirmed by near-zero convergence values for turbulence (k-ε) throughout the entire flow field.

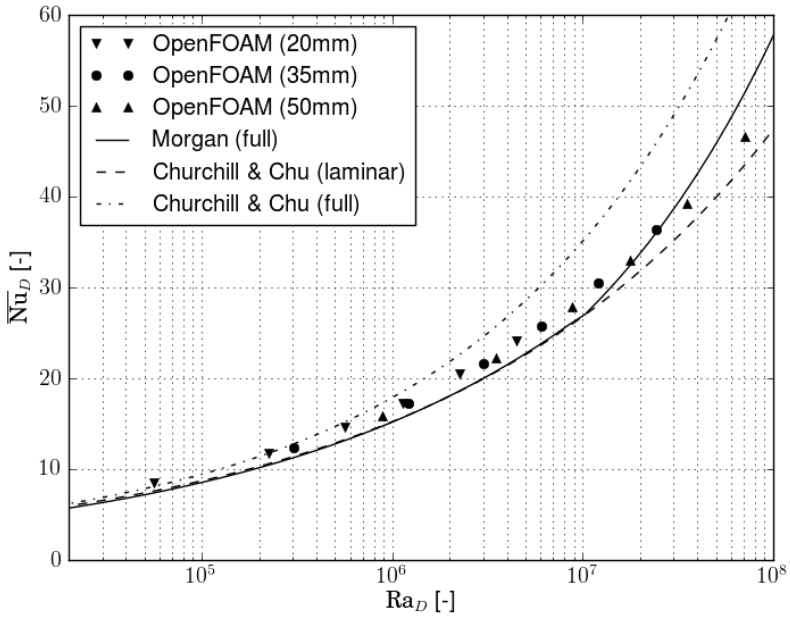

Figure 7: Plot of the average Nusselt number against Raleigh number for OpenFOAM simulations of three cylinder diameters.

One can see the correlation from Morgan *sliding* from well within the laminar range at Ra = 10^7 up to turbulent Nusselt values at Ra ≥ 10^8 while the results from OpenFOAM show no transition to a turbulent regime. The full Rayleigh correlation from Churchill & Chu is significantly influenced by data from the turbulent regime (Ra > 10^9) and shows as such an *upper limit* for any such transition. The case of temperature differences greater than 40K and cylinder diameters greater than 50mm was considered outside that expected in SDHW systems (Logie & Frank, 2009).

Subsequent models defined with multiple regions and varying coordinate schemes (e.g. 3D or 2D axis-symmetric) are currently being investigated for the optimisation of heat transfer and stratification in SDHW tanks. For this a catered OpenFOAM solver was developed that allows simulation of combined heat transfer in solids and fluids under the Boussinesq approximation. As such, complex problems can be defined in which mesh resolution of boundary layers reflect the validation above. Results generated provide insight into system performance and can be compared to this case study. In Figure 8 a time instance from such a 3D simulation is visualised.

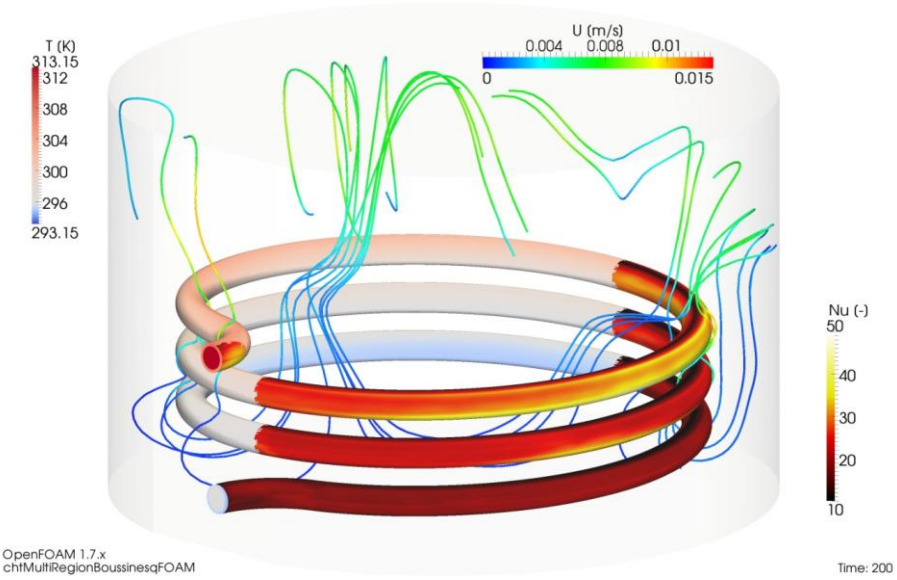

Figure 8: Multi-region (internal and external flow) combined heat transfer (solids and fluids) simulation of an Immersed Heat Exchanger (IHX): 1" pipe (27.2mm inner and 33.7 outer diameter), 70ℓ/h, inlet temperature is 313.15K (top) and the storage temperature at the start of the simulation is 293.15K.

4. Conclusion

The accuracy of the Nusselt numbers as evaluated by OpenFOAM depends significantly on the thickness of the first cell to the cylinder wall. The smaller this cell is, the better the capturing of the temperature gradient interpolated over this cell is, and accordingly the evaluated Nusselt numbers approach those from the laminar correlations of Morgan and Churchill & Chu. If this cell is too small however, the convergence of the flow solution suffers from numerical diffusion in the velocity and pressure field. Due to this compromise, the Nusselt numbers from OpenFOAM are up to 10% higher than the correlations derived from laminar experimental data. It should be noted that the correlations can deviate up to 15% from the experimental data from whence they came.

Another reason why the Nusselt numbers from OpenFOAM lie above those from the laminar correlations stems from the quiescent approximation as defined through the Neumann boundary conditions. They do not necessarily represent a transition to infinite fluid.

Transition from a laminar to turbulent regime can depend on many factors (e.g. temperature difference, geometry and the ratio of heat transfer surface to storage fluid volume). Angular momentum and diffusion effects how the energy introduced into a SDHW is mixed and distributed (stratification into layers of hot and cold) and can therefore not necessarily be ignored, even when laminar regimes predominate.

With numerical inaccuracy in mind one can say that simulations defined in OpenFOAM according to the validation above can predict local heat transfer to within 10% accuracy and tend to underestimate the temperature gradient at surfaces. A *law of wall* for temperature might improve on this.

Calculation time remains a significant limitation to the complexity of models considerable. For the example in Figure 8 in which the mesh consisted of 1.73×10^6 cells and was partitioned onto four 2.66GHz cores (Xeon® X5550), a CPU time of approximately 8 days was required to simulate 200 seconds. As such a simplification of the model and boundary conditions to a 2D axis-symmetric simulation is aimed for in the conclusive stages of this work.

5. References

Churchill, S. W., & Chu, H. H. (1975). Correlating equations for laminar and turbulent free convection from a horizontal cylinder. *Int. Journal of Heat and Mass Transfer , 18*, 1049-1053.

Incropera, F. P., Dewitt, D. P., Bergman, T. L., & Lavine, A. S. (2006). *Fundamentals of Heat and Mass Transfer*. John Wiley & Sons.

Logie, W. R., & Frank, E. (2009). Potential improvement in the design of immersed coil heat exchangers. *ISES Solar World Congress*, (pp. 717-716). Johannesburg.

Morgan, V. T. (1975). The overall convective heat transfer from smooth circular cylinders. In T. E. Hartnett (Ed.), *Advances in Heat Transfer* (Vol. 11, pp. 199-264). New York: Academic Press Inc.

Patel, V. C., Rodi, W., & Scheuerer, G. (1985). Turbulence models for near-wall and low reynolds number flows: a review. *AIAA Journal , 23* (9), 1308-1319.

VDI Gesellschaft Verfahrenstechnik und Chemieingenieurwesen. (2010). *VDI Heat Atlas* (2nd Edition ed.). (V. e. V., Ed.) Düsseldorf: VDI-Verlag GmbH.